Acta Pharmaceutica Sinica B 2025;15(3):1680−1695

Chinese Pharmaceutical Association
Institute of Materia Medica, Chinese Academy of Medical Sciences

Acta Pharmaceutica Sinica B

www.elsevier.com/locate/apsb
www.sciencedirect.com

ORIGINAL ARTICLE

Discovery of a novel polymyxin adjuvant against multidrug-resistant gram-negative bacteria through oxidative stress modulation

Taotao Lu[b,†], Hongguang Han[a,†], Chaohui Wu[a,†], Qian Li[a], Hongyan Hu[c], Wenwen Liu[a], Donglei Shi[a], Feifei Chen[d,e], Lefu Lan[e,f], Jian Li[a,b,g,*], Shihao Song[a,*], Baoli Li[a,*]

[a]*Key Laboratory of Tropical Biological Resources of Ministry of Education and Hainan Engineering Research Center for Drug Screening and Evaluation, School of Pharmaceutical Sciences, Hainan University, Haikou 570228, China*
[b]*State Key Laboratory of Bioreactor Engineering, Shanghai Frontiers Science Center of Optogenetic Techniques for Cell Metabolism, Frontiers Science Center for Materiobiology and Dynamic Chemistry, Shanghai Key Laboratory of New Drug Design, School of Pharmacy, East China University of Science and Technology, Shanghai 200237, China*
[c]*Hainan Hospital of Chinese PLA General Hospital Laboratory Department, Sanya 5720225, China*
[d]*Shanghai Institute of Materia Medica, Chinese Academy of Sciences, Shanghai 201203, China*
[e]*School of Pharmaceutical Science and Technology, Hangzhou Institute for Advanced Study, University of Chinese Academy of Sciences, Hangzhou 310024, China*
[f]*Anhui Province Key Laboratory of Infectious Diseases, the First Affiliated Hospital of Anhui Medical University, Hefei 230022, China*
[g]*Key Laboratory of Xinjiang Phytomedicine Resource and Utilization, Ministry of Education, School of Pharmacy, Shihezi University, Shihezi 832003, China*

Received 12 September 2024; received in revised form 20 November 2024; accepted 23 December 2024

KEY WORDS

Multidrug resistance;
Gram-negative bacteria;
Niclosamide;
Drug repurposing;

Abstract Antibiotic adjuvants offer a promising strategy for restoring antibiotic sensitivity, expanding antibacterial spectra, and reducing required dosages. Previously, compound **15** was identified as a potential adjuvant for Polymyxin B (PB) against multidrug-resistant (MDR) *Pseudomonas aeruginosa* DK2; however, its clinical utility was hindered by high cytotoxicity, uncertain *in vivo* efficacy, and an unclear synergetic mechanism. To address these challenges, we synthesized and evaluated a series of novel

*Corresponding authors.
E-mail addresses: jianli@ecust.edu.cn (Jian Li), songsh@hainanu.edu.cn (Shihao Song), baolili@hainanu.edu.cn (Baoli Li).
[†]These authors made equal contributions to this work.
Peer review under the responsibility of Chinese Pharmaceutical Association and Institute of Materia Medica, Chinese Academy of Medical Sciences.

https://doi.org/10.1016/j.apsb.2025.01.022

Polymyxin B;
Adjuvant;
Broad-spectrum synergism;
Oxidative stress

benzamide derivatives, with **A22** emerging as a particularly promising candidate. **A22** demonstrated potent synergistic activity to PB, minimal cytotoxicity, improved water solubility, and broad-spectrum synergism of polymyxins against various clinically isolated MDR Gram-negative strains. *In vivo* studies using *Caenorhabditis elegans* and mouse models further confirmed the efficacy of **A22**. Moreover, **A22** effectively suppressed the development of PB resistance in *Pseudomonas aeruginosa* DK2. Mechanistic investigations revealed that **A22** enhances polymyxins activity by inducing reactive oxygen species production, reducing ATP levels, increasing NOX activity, and inhibiting biofilm formation, leading to bacterial death. These findings position **A22** as a highly promising candidate for the development of polymyxin adjuvants, offering a robust approach to combating MDR Gram-negative bacterial infections.

1. Introduction

Antibiotic resistance is a significant global public health challenge, complicating the treatment of bacterial infections and leading to increased mortality and morbidity. Recent estimates suggest that approximately 700,000 people die annually from antibiotic-resistant bacterial infections, with projections indicating this number could rise to 10 million by 2050 if no action is taken[1]. The emergence of bacterial resistance has rendered many traditional antibiotics ineffective, further exacerbating the need for novel treatment strategies.

Antibiotic adjuvants, or "antibiotic potentiators", typically lack antimicrobial activity or exhibit minimal inhibition of bacterial growth but enhance the efficacy of antibiotics against resistant bacteria[2-5]. By broadening the spectrum of bacterial coverage and suppressing resistance, adjuvants offer a complementary approach to combating bacterial infections[6,7]. Currently, only a few β-lactamase inhibitor adjuvants (clavulanate, sulbactam, and tazobactam) are available[7], underscoring the urgent need for more diverse adjuvant types.

Pseudomonas aeruginosa (*P. aeruginosa*) is a Gram-negative opportunistic pathogen that causes acute or chronic infection in immunocompromised patients, such as those with cystic fibrosis (CF), cancer, traumas, burns, chronic obstructive pulmonary disease, sepsis, and ventilator-associated pneumonia, including cases related to COVID-19[8,9]. The treatment of *P. aeruginosa* infections is particularly challenging due to its pathogen's rapid mutation rate and capacity to develop resistance to multiple antibiotics[10]. The multidrug-resistant (MDR) *P. aeruginosa* DK2 strain, first isolated from CF patients in 1973, has since evolved into an independent subspecies, significantly increasing morbidity and mortality rates[11]. Our results demonstrated that *P. aeruginosa* DK2 exhibits severe resistance to multiple classes of antibiotics, particularly the last-resort antibiotics Polymyxin B (PB, MIC = 256 μg/mL) and Colistin (MIC >256 μg/mL) (Supporting Information Fig. S1A). Our previous study identified niclosamide (NIC), an anthelmintic drug, as an adjuvant of PB activity against *P. aeruginosa* DK2 and led to the development of a synergistic compound 15 (Fig. 1)[12]. However, compound 15 was limited by high cytotoxicity, uncertain *in vivo* efficacy, and an unclear synergistic mechanism.

In this study, we designed, synthesized, and evaluated a series of derivatives based on compound 15 to improve synergistic potency and druggability, with a focus on derivative **A22** (Fig. 1). It demonstrated significant *in vitro* and *in vivo* synergistic activity to PB against *P. aeruginosa* DK2. Additionally, in combination with PB, derivative **A22** exhibited broad-spectrum antibacterial activity against other clinical drug-resistant Gram-negative bacteria. Mechanistic studies revealed that derivative **A22** enhances PB activity by inducing excessive ROS production, reducing ATP production, increasing NOX activity, and inhibiting biofilm formation, ultimately leading to bacterial death.

2. Materials and methods

The clinical *P. aeruginosa* DK2 isolate was provided by Professor Lars Jelsbak of Technical University of Denmark. *A. Baumannii* 186 and *K. Pneumoniae* 674 isolates were provided by Professor of Min Li of Renji Hospital Affiliated to Shanghai Jiaotong University School of Medicine. *E. Coli* 15,017 was provided by Professor of YouJun Feng, Zhejiang University. *K. Pneumoniae* 15,004, *Proteus mirabilis*, *Enterobacter cloacae* 107, *Enterobacter asburiae* 184, *A. baumannii* 186 and *Serratia arcescens* were provided by Professor Hongyan Hu, Hainan Hospital of Chinese PLA General Hospital. *P. aeruginosa* PAO1 isolate was from ATCC (https://www.atcc.org).

2.1. Synthesis and characterization of *A1−A30*

The details of the synthesis and characterization of **A1−A30** were employed in this manuscript and Supporting Information The purity of all derivatives was determined by HPLC >95% (Supporting Information Table S1). The ^{1}H NMR, HRMS and HPLC spectra for each derivative were provided in Supporting Information Figs. S4−S33.

2.2. Antibiotic efficacy test

The *in vitro* antimicrobial activity of all derivatives/antibiotics was evaluated by the micro broth dilution method, as described previously[12]. In brief, bacterial cultures were diluted with fresh Cation-Adjusted Mueller Hinton broth (CAMHB, BD, CA, USA) to OD_{600} of 0.001. Derivatives/antibiotics were 2-fold serially diluted in bacterial cultures in the 96-well plate and incubated with equal volumes of inoculum for 18 h at 37 °C. Then, MIC values were measured by recording the optical density at 600 nm (OD_{600}) of each well using BioTek Synergy 2 (BioTek, VT, USA). MIC values were recorded as the lowest concentration required to achieve 100% growth inhibition compared to growth in untreated wells.

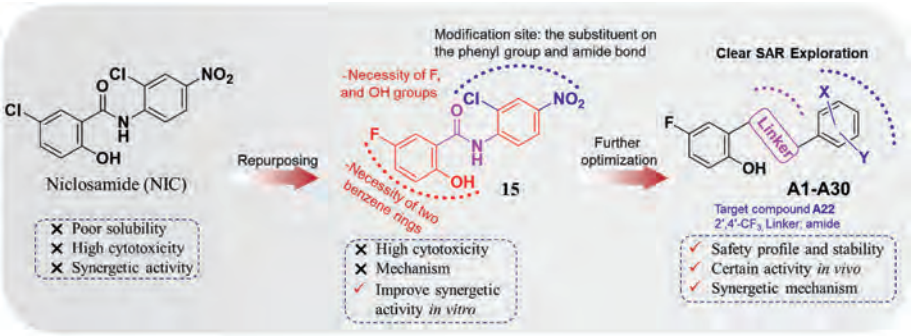

Figure 1 Structural design and optimization strategy.

2.3. *Chessboard assay*

In vitro synergetic activity was evaluated in 96-well plates by the checkerboard microdilution method. In brief, bacterial cultures were diluted with fresh CAMHB (BD) to OD_{600} of 0.001 and were plated in a 96-well culture plate at 100 μL/well. Antibiotics and derivatives to be measured were added to the 96-well plate, and the checkerboard method was used for determination. The concentration range was 0.25−32 μg/mL, and the final concentration range of derivatives was 5−100 μmol/L (continuous 2-fold change). The plates were incubated at 37 °C for 18 h and measured by optical density at OD_{600}. The value of FIC was calculated as Eq. (1):

$$\text{FIC} = [\text{MIC of the agents in combination}]/[\text{MIC of the agent alone}] \quad (1)$$

The FICI is the sum of the FICs of the derivatives and antibiotics.

2.4. *Time-kill assay*

The detailed method for time-kill assay was previously described[12].

2.5. *Mammalian cytotoxicity*

Cells were seeded in 96-well plates at 10,000 cells per well in a total volume of 100 μL of media containing 10% serum. Serially diluted compounds in 10 μL of media were added to the cells 24 h later. After 1 day of incubation, Cell Counting Kit-8 reagents (CCK8, Yeasen, Shanghai, China) were added, and luminescence was measured according to the manufacturer's instructions. Cell viability was measured by CCK8 assay of 293 T and HUVEC cells line. The data are presented as a percentage of viable cells with vehicle-treated cells set as 100.

2.6. *Water solubility assay*

The derivative was dissolved in HPLC-grade methanol and diluted in a gradient to 0.56, 0.28, 0.14, 0.07, 0.035, 0.018, 0.0088, 0.0044, 0.0022, and 0.0011 mg/mL of the solution. The UV absorption peak area in 254 nm was measured by HPLC to construct the concentration−UV absorption area standard curve. Add an excess of the derivatives into water to form a supersaturated solution. After stirring for 24 h, the UV absorption peak area in 254 nm was measured by HPLC, and then the water solubility value of the derivative was calculated from the previous standard curve.

2.7. *Plasma protein binding assay*

This experiment was outsourced to Pharmalegacy Laboratories Co., Ltd. (Shanghai, China). Briefly, aliquots of 100 μL of blank dialysis buffer were applied to the receiver side of the dialysis chambers. Then 100 μL of the plasma spiked with test compounds was applied to the donor side. Preparing T_0 plasma samples for initial concentrations. Aliquot 25 μL of the plasma spiked with test and reference compounds was added to the 96-well sample preparation plate as T_0 plasma samples. The samples were added blank buffer. Quench the samples with 200 μL of acetonitrile containing internal standard. Cover the dialysis block with a plastic lid and place the entire apparatus for 5 h at 37 °C. After 5 h of incubation, aliquots of 25 μL were taken from both the donor and receiver sides of the dialysis apparatus and transferred into new sample preparation plates. Each aliquot was then mixed with an equal volume of the opposite matrix (blank buffer for plasma and plasma for blank buffer). Quench the samples with 200 μL acetonitrile containing internal standard. Vortex all the samples at 500 rpm for 10 min followed by centrifugation at 4000×*g* for 10 min. The transfer of 100 μL of the supernatants to a new 96-well plate and mix the samples with 200 μL of Milli-Q water. Cover the sample plate and store it in a freezer (−20 °C) until LC−MS/MS analysis.

2.8. *hERG channel Qpatch assay*

This experiment was commissioned by the ion channel platform of Shanghai Institute of Materia Medica, Chinese Academy of Sciences (Shanghai, China). The inhibitory activity of test compounds on hERG potassium channels was tested in CHO-hERG cells, which were cultured in 175 cm^2 culture flasks. Cell density was ranged within 2×10^6−5×10^6 cells/mL. The single-cell high-impedance sealing and whole-cell pattern formation processes are automatically completed by the Qpatch instrument. After acquiring whole-cell recording mode, cells were clamped at −80 mV. The voltage stimulation was applied every 15 s and recorded for 2 min, and the extracellular fluid was administered for 5 min, and then the administration process was started. Each test concentration was given for 2.5 min starting from low concentrations to high concentrations. Cisapride was used as a positive control.

2.9. Stability test in liver microsomes assay

Compounds were incubated with human, or mouse liver microsomes and reduced nicotinamide adenine dinucleotide phosphate in 0.05 mol/L phosphate buffer (pH = 7.4) at 37 °C for 0−60 min. The reaction was quenched, and the amount of the remaining compound was analyzed using liquid chromatography-tandem mass spectrometry (LC−MS/MS).

2.10. The human CYP450 enzymes inhibition assay

This experiment was outsourced to Pharmalegacy Laboratories Co., Ltd. (Shanghai, China). The reaction was initiated by the addition of the coenzyme NADPH (6.5 mmol/L). Prepare probe substrate and HLM/MLM mixture in a 96-well plate according to the appropriate proportion. Probe substrate (318 μL) and human liver microsome mixture were dispensed to the incubation plates. Then add 2 μL of 8 serial concentration levels, and then add 80 μL aliquot of the NADPH regenerating system as 0 min to initiate the reaction. The sample plates were incubated at 37 °C and started a timer. The assay plates for testing inhibition of different CYP isoforms were incubated for different periods of time: 10 min for 1A2, 2B6, 2C8, 2C9, 2D6, and 3A4; 40 min for 2C19). At time points, 100 μL incubation solution was transferred to the wells of the corresponding plates containing 300 μL of internal standard solution, respectively, to stop the reaction. After quenching, shake the plates for 10 min and centrifuge the samples at 3000×*g* for 15 min, and 100 μL of the supernatant was transferred from each well to a 96-well sample plate containing 300 μL of water for LC−MS/MS analysis.

2.11. C. elegans liquid medium killing and rescue assay

Wild-type *C. elegans* (N2) strains were obtained from Caenorhabditis Genetics Center (MN, USA). The age-synchronized L4 larvae were transferred and incubated on peptone-glucose-sorbitol (PGS) agar plates (containing PAO1 strain) for 24 h at 20 °C. PAO1 trains cells at midlogarithmic phase (OD_{600}∼0.5) were harvested and diluted with S-Buffer to OD_{600} of 2, then 2 mL of bacterial solution was added to PGS agar plates. Infected N2 worms were washed with M9 buffer, resuspended, and then washed again with M9 buffer (1 L ddH_2O, 5 g NaCl, 6 g Na_2HPO_4. 3 g KH_2PO_4, and 1 mL 1 mol/L $MgSO_4$). Approximately 20 worms were transferred to 24-well plates (containing compounds to be tested or not, and 0.2 mmol/L floxuridine to prevent the worms from spawning). The number of worms (live or dead) was recorded every day.

2.12. Mice infection assay

A murine wound infection model in BALB/c female mice (6−8 week, 20−22 g) was established, and healthy mice were provided by Biotechnology Co., Ltd. (Guangzhou, China). Derivative **A22** was dissolved in saline containing 0.1% Tween 80 and PB was prepared in saline. First, mice were anesthetized with 4% chloral hydrate and then shaved on the back. A ∼5 mm wound was created on the back of the mice and then 30 μL of *P. aeruginosa* DK2 (5×10^8 CFU) was inoculated on the surface of the wound. Surrounded by 48 h of wound infection, the wound was treated with saline, PB alone, or PB in combination with derivative **A22**, respectively. The drugs were administered twice a day. Then, a homogenate of the skin at the wound site was prepared and the bacterial density was determined CFU counting was obtained on an agar plate. Meanwhile, the wounds and body weights of the mice were monitored daily. After Day 5, the surviving mice were euthanized by cervical dislocation. Wounds were removed and homogenized in sterile PBS for bacterial loading. All experimental procedures were executed according to the protocols approved by the Hainan University Animal Research Committee (SYXK2023-0031).

2.13. Resistance assay

The detailed method for resistance assay was previously described[12]. Briefly, the ability of the combination of PB and derivative **A22** to suppress resistance development was determined by serial passaging. *P. aeruginosa* DK2 with approximately OD = 0.01 was grown in 3 mL of LB broth with a sub-MIC (1/2 MIC) concentration of PB alone or in combination with derivative **A22**. At 24 h intervals, the cultures were assessed for growth. A bacterial dilution was made by using the bacteria from the sub-MIC concentration of PB (1/2 MIC). Then, the concentration of these bacteria was adjusted to OD = 0.01 and subjected to the next MIC assay. The tubes were incubated at 37 °C for 24 h. For the PB and **A22** combination group, the concentration of derivative **A22** was kept constant at 10 μmol/L throughout the experiment. This serial passaging was repeated for 14 days, and the fold change in the MIC value was determined.

2.14. qPCR analysis assay

Bacterial cells were cultured at 37 °C in LB broth to the logarithmic-growth phase (OD_{600} = 1.0). Cells were collected by centrifugation, and total RNA was extracted using an Eastep Super Total RNA Extraction Kit (Hlingene, Shanghai, China). cDNA synthesis was performed using a Hifair III One Step RT-qPCR SYBR Green Kit (Yeasen, Shanghai, China). Primers for RT-qPCR were listed in Supporting Information Table S2. The RT-qPCR (Thermo Fisher, QuantStudio™ 1, MA, USA) experiments were performed on a Hieff qPCR SYBR Green Master Mix (Yeasen, Shanghai, China). The relative expression levels of the target genes were calculated using the comparative CT ($2^{-\Delta\Delta CT}$) method[13].

2.15. Oxidative stress sensitivity measurement

Dilute the bacteria to 0.01 and treat the bacteria with compounds. When the OD_{600} of the bacteria reaches 1.0, collect 3 mL of bacteria liquid, and resuspend and centrifuge (JIDI, JIDI-21 R, Guangzhou, China) with 1 mL of sterile 1 × PBS buffer. Then, PBS containing 0.2 mol/L H_2O_2 was added to resuspend the organisms, and constant temperature was shaken for 15 min at 37 °C. Afterward, the number of DK2 strains was determined by the gradient dilution coated plate method and plate colony counting method. The suspension of test bacteria was diluted 10^1−10^7 times using sterile 1 × PBS, respectively, and 5 μL of the diluted suspension was taken in LB solid medium spot plates, which were incubated at 37 °C in an incubator for days 1−2, after the number of colonies on the plates was counted and recorded, and the CFU to analyze the susceptibility to oxidative stress[14].

2.16. Bacterial ATP level assay

The ATP content in bacteria was detected by Solarbio ATP Content Detection Kit (Solarbio, BC0300, Beijing, China), and the strains were treated with the compounds singly and in combination, when OD_{600} = 1.0, 2 mL of bacterial liquid was collected and centrifuged, 1 mL of extraction solution was added, and ultrasonically crushed in an ice bath, and then ATP was extracted from bacteria according to the instructions, and put on the ice to be measured. The samples were added into 96-well plates according to the instructions, and after mixing thoroughly, the absorbance value A1 at 340 nm for 10 s was measured immediately, and then the 96-well plates were placed in an incubator at 25 °C for 3 min, and then the absorbance value A2 at 3 min for 10 s was measured immediately. The relative ATP levels was calculated[15].

2.17. Intracellular NADH oxidase assay

The NADH oxidase (NOX) content in bacteria was assayed using the Solarbio NOX activity assay kit (Solarbio, BC0630, Beijing, China). The strains were treated with the compounds singly and in combination, and 1 mL of the bacteria was collected when OD_{600} = 1.0, and the NOX activity was measured by the extraction method according to the instructions of the kit. Calculate the relative NOX activity[16].

2.18. Intracellular ROS detection

In this experiment, a Beyotime reactive oxygen detection kit (Beyotime, S0033S, Shanghai, China) was used, bacteria were treated with the drug, and the organisms were collected, DCFH-DA was diluted according to 1:1000, so that the final concentration was 10 μmol/L. The organisms were collected and suspended in diluted DCFH-DA, incubated at 37 °C for 20 min; the organisms were resuspended with LB medium, and then centrifuged at 5000 rpm (JIDI-21 R) for 5 min, and washed to remove the DCFH-DA that had not entered into the cells. The organisms were centrifuged at 5000 rpm (JIDI-21 R) for 5 min, washed, and the DCFH-DA that did not enter the cells was removed. 488 nm excitation wavelength and 525 nm emission wavelength were used for the zymography detection[17].

2.19. Biofilm production assay

Single colonies were inoculated in LB culture solution and cultured overnight at 37 °C and 200 rpm (MIULAB, ES-60 E, Hangzhou, China). Determine the OD_{600} value of the bacterial liquid and dilute the bacterial liquid with LB until OD_{600} = 0.01. The diluted bacterial solution was treated by compounds alone and combined with polymyxin B respectively. Bacterial cells were inoculated 1:100 in CPG medium in 96-well polystyrene plates. After incubation at 37 °C for 24 h, the cells were stained with 0.1% crystal violet (CV) for 30 min. The planktonic cells were removed by several rinses with H_2O. The CV-stained bound cells were air dried for 1 h and then dissolved in 95% ethanol, and the optical density at 570 nm (OD_{570}) of the solution was measured to quantify biofilm formation[18].

2.20. Confocal laser scanning microscopy assay

Cover glass was placed in a six-well plate, and the strain was treated with the compound. The biofilms formed on the coverslips were washed three times with PBS (pH 7.2) and then dried at 60 °C for 30 min. The biofilms were stained with a 0.01% acridine orange (Macklin, 65-61-2, Shanghai, China) and ethidium bromide solution (Macklin, 25,535-16-4, Shanghai, China) for 15 min and observed by confocal laser scanning microscopy (Olympus, FV3000, Japan)[19].

2.21. RNA-seq analysis assay

Total RNA was extracted from *P. aeruginosa* DK2 by using the Eastep Super Total RNA Extraction Kit. RNA purity was detected by using the Nano Photometer spectrophotometer (Bio-DL, Mico Drop Shanghai, China), RNA concentration was measured by using Qubit RNA Assay Kit in Qubit 2.0 Fluorometer (Thermo Fisher, Qubit 2.0, MA, USA), and RNA integrity was assessed by using the RNA Nano 6000 Assay Kit with the Bioanalyzer 2100 system (Agilent Technologies, 2100 system, CA, USA). Sequencing libraries were generated by using the NEB. Next, Ultra Directional RNA Library Prep Kit for Illumina (NEB, E7760S, MA, USA). Finally, the products were purified (Beckman Coulter, AMPure XP system, CA, USA), and library quality was assessed on the Agilent Bioanalyzer 2100 system. Clustering of the index-coded samples was performed on a cBot Cluster Generation System using TruSeq PE Cluster Kit v3-cBot-HS (Illumina, CA, USA). After cluster generation, the library preparations were sequenced on an Illumina HiSeq platform, and paired-end reads were generated. Trimmed sequence reads were aligned to the *P. aeruginosa* DK2 genome sequence using Bowtie2-2.2.3, and normalized read counts were compared using HTSeq v0.6.1 as described previously. Then, the FPKM of each gene was calculated based on 26 reads of the gene, and the read count was mapped for each gene[20,21].

2.22. Statistical analysis

Statistical analyses were performed with GraphPad Prism 8. The data are presented as the means ± standard deviation (SD). Asterisks in the figures indicate corresponding statistical significance.

3. Results and discussion

3.1. Design and chemistry

Building on the structure−activity relationship (SAR) insights from NIC and compound 15, we identified that the presence of two benzene rings and the 2-hydroxyl and 5-fluoro substitutions on the left benzene ring were crucial for synergistic potency[12,22]. Modifications, including the introduction of new linkers and substituents on the right benzene ring, were modulated to enhance synergistic activity, reduce cytotoxicity, and improve druggability (Fig. 1).

A range of linker types, including sulfonamide, urea, and hydrazide amide, were introduced to modulate electronic and steric properties. Besides, research has shown that incorporating additional carbon atoms and amino acid linkers can enhance the flexibility and pharmacokinetic profiles of compounds[23]. Then, various bulky bis-amide linkers were inserted into the benzene rings. Moreover, substituents were strategically introduced at different positions on the right benzene ring. Electron-withdrawing groups (*e.g.*, trifluoromethyl, nitro, etc.) and

electron-donating groups (*e.g.*, methoxy, hydroxyl, etc.) were introduced at the ortho, meta, and para positions to modulate electronic properties, enhance synergistic potential and minimize mammalian cytotoxicity. The synthesis of compounds **A1**−**A30** was accomplished as depicted in Schemes 1−4.

Specifically, the synthesis of target derivatives **A1**−**A4** is depicted in Scheme 1. The intermediate **M1** was synthesized *via* a nucleophilic substitution starting from commercially available 5-fluoro-2-methoxybenzenesulfonyl chloride (**1**). **M1** was then reacted with commercially available 2-chloro-1-fluoro-4-nitrobenzene (**4**) in the presence of potassium carbonate, yielding intermediate **M2**. Concurrently, commercially available 5-fluoro-2-methoxyaniline (**2**) was treated with triphosgene and triethylamine to generate isocyanic acid, which was subsequently reacted with 2-chloro-4-nitroaniline (**3**) to give the urea intermediate **M3**. Intermediate **M4** was obtained through the nucleophilic substitution reaction of **4**, followed by condensation with commercially available 5-fluoro-2-methoxybenzoic acid (**20**) to give the intermediate **M5**. Additionally, commercially available 2-(5-fluoro-2-methoxyphenyl)acetic acid (**5**) underwent a condensation with **3** to produce the intermediate **M6**. Finally, demethylation of the key intermediates, **M2**, **M3**, **M5**, and **M6**, produced derivatives **A1**−**A4**, respectively.

The synthesis of compounds **A5**−**A15** is shown in Scheme 2. Using PCl_3 as the acylating agent, various commercially available substituted amino acids (**6**−**16**) were coupled with **3** to produce intermediates **M7**−**M17**. These intermediates were then deprotected from Fmoc in the presence of piperidine in acetonitrile to generate intermediates **M18**−**M28**. Condensation of intermediates **M18**−**M28** with **20** in the presence of EDCI produced

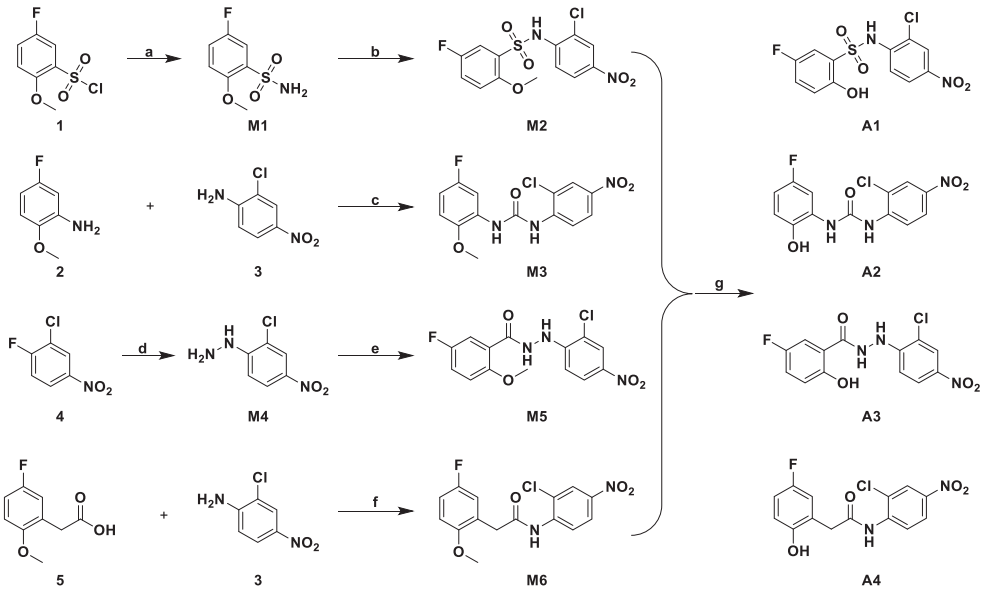

Scheme 1 Synthesis routes of derivatives **A1**−**A4**. Reagents and conditions: (a) $NH_3{\bullet}H_2O$, EtOH, 80 °C, 1 h; (b) 2-chloro-1-fluoro-4-nitrobenzene, K_2CO_3, DMSO, 100 °C, 12 h; (c) (1): triphosgene, Et_3N, THF, 0 °C, 1 h; (2): 2-chloro-4-nitroaniline, THF, 3 h; (d) $N_2H_4{\bullet}H_2O$, 1,4-dioxane, 60 °C, 1 h; (e) 5-fluoro-2-methoxybenzoic acid (**20**), EDCI, HOBt, DCM, r.t., 12 h; (f) PCl_3, toluene, 110 °C, 12 h; (g) BBr_3, DCM, 0 °C−r.t., 3 h.

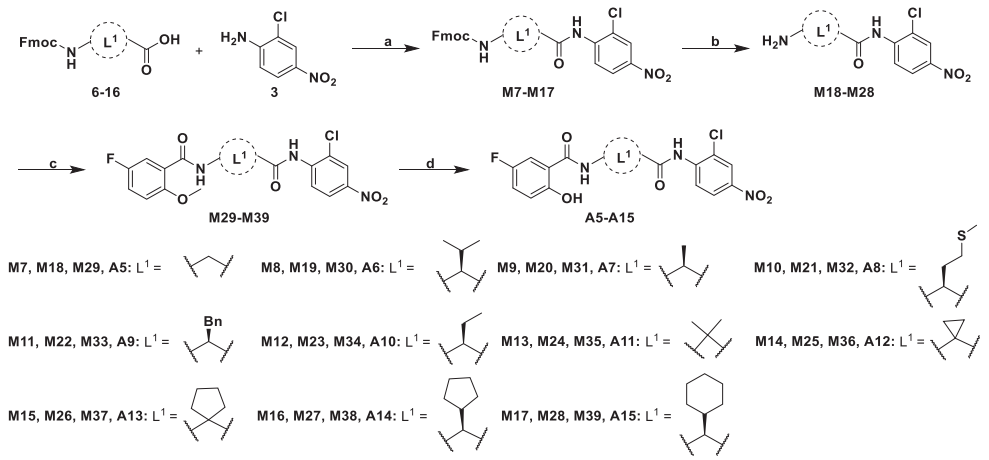

Scheme 2 Synthesis routes of target derivatives **A5**−**A15**. Reagents and conditions: (a) PCl_3, toluene, 110 °C, 1 h; (b) Piperidine, ACN, r.t., 12 h; (c) **20**, EDCI, DMAP, DCM, r.t., 12 h; (d) BBr_3, DCM, 0 °C−r.t., 3 h.

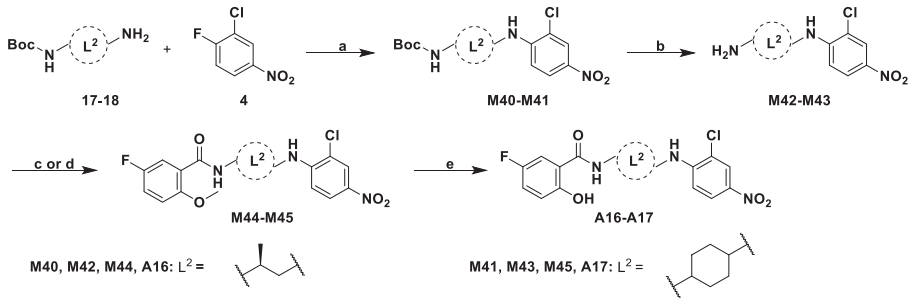

Scheme 3 Synthesis routes of target derivatives **A16**−**A17**. Reagents and conditions: (a) DIPEA, DMSO, 80 °C, 3 h; (b) TFA, DCM, r.t. 3 h; (c) For **M44**, **20**, EDCI, DMAP, DCM, r.t., 12 h; (d) For **M45**, **20**, EDCI, HOBt, DCM, r.t., 16 h; (e) BBr_3, DCM, r.t., 3 h.

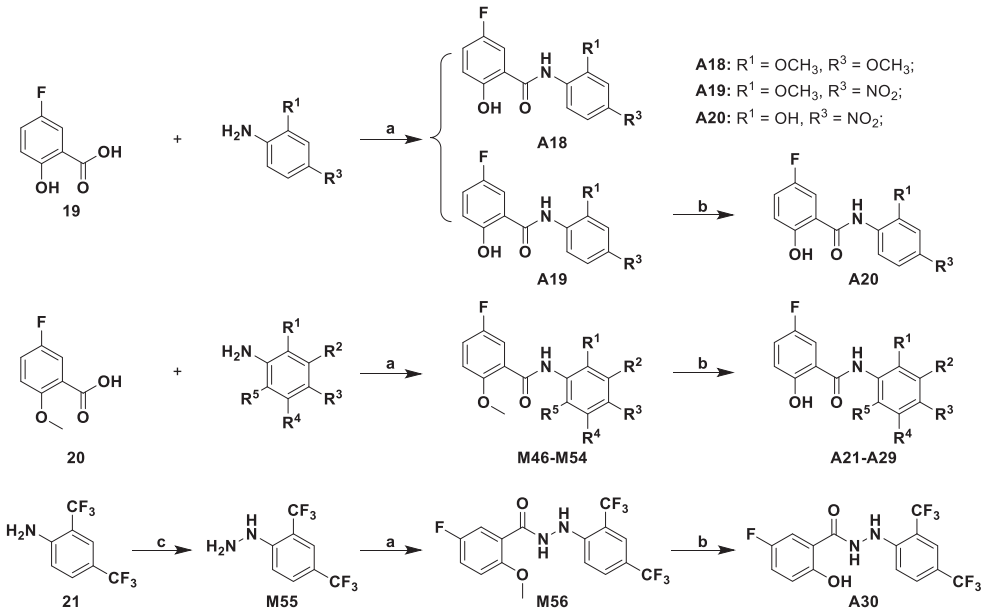

Scheme 4 Synthesis routes of target derivatives **A18**−**A30**. Reagents and conditions: (a) PCl_3, toluene, 110 °C, 12 h; (b) BBr_3, DCM, r.t.; 3 h (c) $NaNO_2$, $SnCl_2$, conc. HCl, r.t., 3 h.

M29−**M39**, which were subsequently demethylated using BBr_3 to afford the corresponding derivatives **A5**−**A15**.

As shown in Scheme 3, intermediates **M40**−**M41** were prepared by nucleophilic substitution of **4** with various substituted amines, followed by deprotecting the BOC group using trifluoroacetic acid to yield intermediates **M42**−**M43**. Condensation of intermediates **M42**−**M43** with **20** in the presence of EDCI and DMAP or HOBt produced intermediates **M44**−**M45**, respectively, which were then demethylated using BBr_3 to afford the corresponding derivatives **A16**−**A17**.

As described in Scheme 4, the direct coupling of commercially available 5-fluoro-2-hydroxybenzoic acid (**19**) and 2,4-dimethoxyaniline afforded the derivative **A18**. Derivative **A19** was accessed under similar coupling conditions by condensation of **19** with 2-methoxy-4-nitroaniline, followed by demethylation with BBr_3 to yield derivative **A20**. Commercially available 2,4-bis(trifluoromethyl)aniline reacted with sodium nitrite in the presence of $SnCl_2$ and concentrated HCl to give hydrazine intermediate **M55**. Subsequent condensation of the intermediate **M55**, or various substituted aniline, with **20** yielded intermediates **M46**−**M54** and **M56**, respectively, which were then subjected to demethylation using BBr_3 to give derivatives **A21**−**A30**.

3.2. Evaluation of derivatives for antibacterial activity against P. aeruginosa DK2

Adjuvants were typically defined as compounds that lack direct antimicrobial activity or exhibit minimal inhibition of bacterial growth but enhance the inhibitory effect of antibiotics[7]. Therefore, all target derivatives **A1**−**A30** were evaluated for their *in vitro* antibacterial activity against *P. aeruginosa* DK2 using the broth-dilution method. The minimum inhibitory concentration (MIC)

was determined as the concentration at which there was approximately 100% reduction in bacterial growth compared to the drug-free control. The antibacterial activity results were tabulated in Tables 1 and 2. As expected, the majority of the derivatives were inactive against *P. aeruginosa* DK2, with MIC values exceeding 1000 μmol/L. Only compounds **A3**, **A20**, **A25**, and **A28**−**A30** demonstrated moderate antibacterial activity, with MIC values ranging from 50 to 100 μmol/L.

Table 1 Structures and synergistic activity of the lead compound **15** and derivatives **A1**−**A17**.

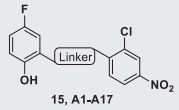

15, A1-A17

Compd.	Linker	MIC[a]		FICI[b]
		Derivative alone	Combination (Compd./PB)	
15		>1000	10/1	0.014
A1		>1000	100/2	0.108
A2		>1000	100/4	0.115
A3		50	10/1	0.204
A4		>1000	100/1	0.029
A5		>1000	100/4	0.116
A6		>1000	100/1	0.104
A7		>1000	100/2	0.108
A8		>1000	100/>32	NT[c]
A9		>1000	100/>32	NT[c]
A10		>1000	10/16	0.073
A11		>1000	10/16	0.073
A12		>1000	10/16	0.073
A13		>1000	10/4	0.026
A14		>1000	10/4	0.026
A15		>1000	10/4	0.026
A16		>1000	10/32	0.128
A17		>1000	100/>32	NT[c]

[a]MIC: minimum inhibitory concentration; Unit of derivatives is μmol/L, and unit of PB is μg/mL;

[b]FICI: fractional inhibitory concentration index. The MIC of PB alone against *P. aeruginosa* DK2 is 256 μg/mL; when derivatives alone MIC >1000 μmol/L, FICI is calculated according to 1000 μmol/L;

[c]NT: unmeasured.

Table 2 Structures and synergistic activity of derivatives **A18**−**A30**.

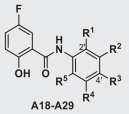

A18-A29

Compd.	R^1	R^2	R^3	R^4	R^5	MIC[a]		FICI[b]
						Derivative alone	Combination (Compd./PB)	
A18	OCH_3	H	OCH_3	H	H	>1000	100/>32	NT[c]
A19	OCH_3	H	NO_2	H	H	>1000	10/2	0.018
A20	OH	H	NO_2	H	H	100	25/2	0.258
A21	CF_3	H	CN	H	H	>1000	10/2	0.018
A22	CF_3	H	CF_3	H	H	>1000	10/1	0.014
A23	H	CF_3	H	CF_3	H	>1000	10/4	0.026
A24	Cl	H	CF_3	H	H	>1000	10/8	0.041
A25	CF_3	H	NO_2	H	H	100	10/1	0.104
A26	NO_2	H	SO_2CF_3	H	H	>1000	10/2	0.018
A27	H	H	SO_2CF_3	H	H	>1000	10/2	0.018
A28	CF_3	H	NO_2	H	Cl	100	10/1	0.104
A29	CF_3	H	CF_3	H	NO_2	100	10/2	0.108
A30	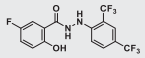					100	10/2	0.108

[a]MIC: minimum inhibitory concentration; Unit of derivatives is μmol/L, and unit of PB is μg/mL;

[b]FICI: fractional inhibitory concentration index. The MIC of PB alone against *P. aeruginosa* DK2 is 256 μg/mL; when derivatives alone MIC >1000 μmol/L, FICI is calculated according to 1000 μmol/L;

[c]NT: unmeasured.

3.3. Evaluation of derivatives for synergistic activity to PB against P. aeruginosa DK2 and SAR study

The synergistic activity of derivatives was assessed using the checkerboard microdilution assay. The synergistic effects were evaluated by the fractional inhibitory concentration (FICI), with synergism defined as a FICI ≤ 0.5[24]. The FICI was calculated by summing the ratios with the MIC of each drug in combination to the MIC of the drug when used individually. As shown in Table 1, derivatives **A1**−**A3**, incorporating sulfonamide, urea, and hydrazide amide linkers, demonstrated a reduction in synergistic activity (FICI range: 0.108−0.204) compared to the lead compound 15 (FICI = 0.014). Notably, derivative **A3** (10 μmol/L), featuring a novel amido hydrazine linker, significantly improved the MIC of PB from 256 to 1 μg/mL, below the clinical sensitivity threshold (MIC $\leq$2 μg/mL). However, **A3** exhibited weak antibacterial activity against *P. aeruginosa* DK2, with a MIC of 50 μmol/L (16.28 μg/mL), raising concerns about potential drug resistance after long-term usage. Derivatives **A4**−**A17** exhibited synergistic activity against *P. aeruginosa* DK2 at concentrations of 10−100 μmol/L (FICI = 0.026−0.204). Unfortunately, none surpassed the performance of 15. The results indicated that the introduction of sulfonamide, urea, various diamine, and amino acid linkers led to a reduction in synergetic activity. Additionally, derivatives with bulky linkers (**A6**, **A10**−**A11**) were explored and resulted in a complete loss of synergetic activity (MIC of PB > 32 μg/mL). Overall, the amide linker was found to be crucial for maintaining synergetic activity.

Due to the weak potency observed, further optimization of the linker moiety was not pursued. Subsequently, our focus shifted to examining the impact of substitutions on the right benzene ring (Fig. 1). To explore the effects of introducing various electron-withdrawing and electron-donating groups, derivatives **A18**−**A30** were synthesized and evaluated (Table 2). Initially, derivative **A18**, featuring a 2′−OCH_3-4′−OCH_3 substitution, led to a significant loss of synergistic activity. Additionally, the 2′−Cl substituent was replaced with 2′−OCH_3 or 2′−OH to yield derivatives **A19**−**A20**, both of which exhibited limited potency (FICI = 0.018 and 0.258, respectively). This suggests that the introduction of electron-donating groups adversely affects synergistic activity. Further exploration with various electron-withdrawing substituents (**A21**−**A29**), such as −CF_3, −CN, −SO_2CF_3, and −NO_2 revealed improved synergistic activity (FICI <0.5) across all derivatives. Notably, electron-

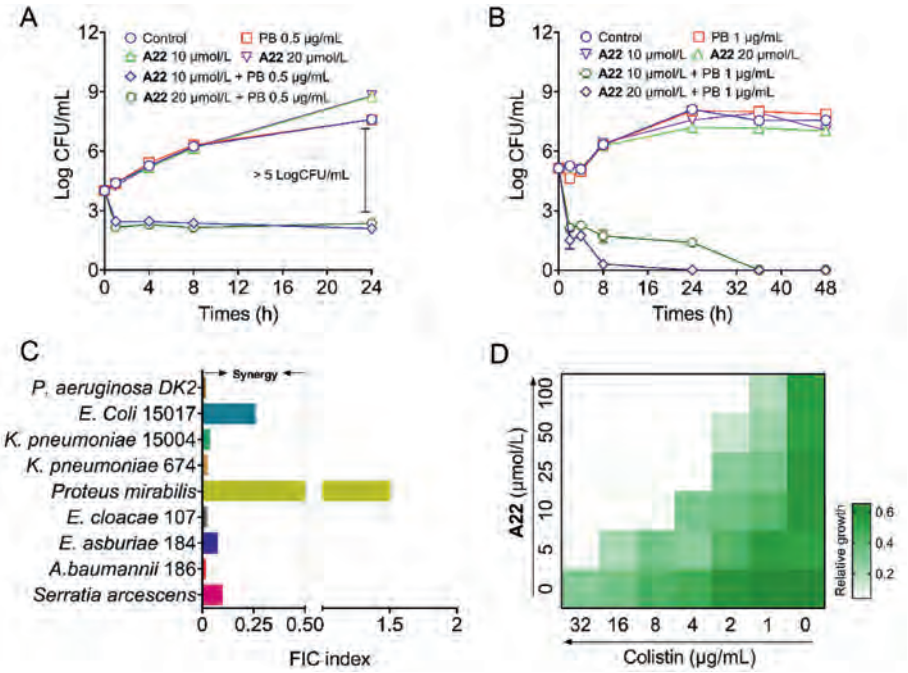

Figure 2 **A22** synergized the efficacy of polymyxins against MDR Gram-negative bacteria. (A, B) Time-kill curves of **A22** and PB, used alone or in combination; (C) Synergetic activity of **A22** in combination with PB against diverse species of clinical MDR Gram-negative bacteria; (D) Effect of **A22** in combination with Colistin on synergetic activity against *P. aeruginosa* DK2.

withdrawing substitutions at the 2′,4′-position exerted favorable effects on activity. Among these, derivative **A22**, with bis(trifluoromethyl) substitution, maintained potency (FICI = 0.014) comparable to lead compound 15, enhancing the MIC of PB from 256 to 1 μg/mL, while itself exhibiting no inhibitory activity against *P. aeruginosa* DK2 (MIC >1000 μmol/L). Conversely, derivative **A23**, with 3′,5′-bis(trifluoromethyl) substitution, demonstrated lightly reduced synergetic activity (FICI = 0.026) compared to **A22**. These results suggested that 2′,4′-substitution with electron-withdrawing groups played a crucial role in modulating synergetic activity. Further substitutions, including replacing the 4′-NO_2 group with 4′−CN (**A21**), 4′−CF_3 (**A24**), and 4′−SO_2CF_3 (**A26**−**A27**), as well as replacing 2′−Cl with 2′−CF_3 (**A25**), collectively resulted in a reduction in synergistic activity. Derivatives **A28** and **A29** demonstrated synergistic activity comparable to compound 15, yet at 100 μmol/L, they exhibited inhibitory activity against *P. aeruginosa* DK2. Finally, using the pharmacophore confluence strategy, from the most potent derivatives, **A3** (linker) and **A22** (substitutions), derivative **A30** was synthesized. However, it still demonstrated some antibacterial activity, along with a decrease in synergistic activity (FICI = 0.108). Based on these findings, **A22** was selected for further investigation to determine its potential to overcome the limitations of lead compound 15 and establish itself as a promising adjuvant candidate.

3.4. *Derivative **A22** as a potent adjuvant from time-kill assay*

To further elucidate the synergistic effects of derivative **A22** to PB, time-kill curves were determined. The results confirmed that neither **A22** (10 μmol/L = 3.67 μg/mL, or 20 μmol/L = 7.34 μg/mL) nor PB (0.5 or 1 μg/mL) significantly affected bacterial growth when used alone. However, a substantial reduction in colony-forming units (CFUs) as early as 2 h when **A22** was combined with PB (Fig. 2A and B). Moreover, the combination of **A22** (10 or 20 μmol/L) with PB (1 μg/mL) completely inhibited bacterial growth at 36 or 24 h, respectively (Fig. 2B), outperforming the lead compound 15 (Fig. S1B). These results are consistent with the checkerboard assay findings, suggesting that **A22** was a potent adjuvant for enhancing the efficacy of PB against *P. aeruginosa* DK2.

Table 3 Cytotoxicity, solubility and PPB of compounds **15** and **A22.**

Compd.	293 T[a] IC_{50} (μmol/L)	HUVEC[b] IC_{50} (μmol/L)	Solubility (μg/mL)	PPB (h, %)[d]
15	12.11	18.69	< LOD[c]	96.86
A22	150.50	>200	4.0	97.94

[a]293 T: human embryonic kidney cell lines.
[b]HUVEC: human umbilical vein endothelial cell lines.
[c]LOD: limit of detection.
[d]PPB: percent of plasma protein binding in human serum.

3.5. *Derivative **A22** as a potent broad-spectrum antibiotic adjuvant to polymyxins*

To evaluate the broader applicability of **A22** in combination with PB against various MDR Gram-negative bacteria, we assessed the FICI values for eight species of bacteria: *Acinetobacter baumannii (A. baumanni)* 186, *Klebsiella pneumoniae (K. pneumoniae)* 674, *K. pneumoniae* 15,004 (resistant to all antibiotics used clinically), *Enterobacter asburiae (E. asburiae)* 184, *Escherichia coli (E. coli)* 15,017, *Enterobacter cloacae (E.* cloacae*)* 107, *Proteus mirabilis*, and

Table 4 Liver microsome metabolic stability of **A22** in human and mice.

Compd.	HLM[a]		MLM[a]	
	$t_{1/2}$[b] (min)	Remaining (t = 1 h)	$t_{1/2}$[b] (min)	Remaining (t = 1 h)
Verapamil	27.53	22.05%	11.41	2.19%
A22	29.09	23.96%	54.43	46.31%

[a]HLM: human liver microsome stability, MLM: mice liver microsome stability.
[b]$t_{1/2}$: half-life.

Table 5 Inhibitory effects of **A22** on CYP450 enzyme family.

Inhibition for CYP isoforms (IC_{50}, μmol/L)[a]							
Compd.	1A2	2B6	2C8	2C9	2C19	2D6	3A4
Inhibitors[b]	0.02	0.05	1.74	0.16	0.74	0.03	0.01
A22	6.13	>33.00	2.61	0.29	20.53	1.88	>33.00

[a]IC_{50} values for CYPs.
[b]Reference inhibitors include α-naphthoflavone for 1A2, ticlopidine for 2B6, quercetin for 2C8, sulfaphenazole for 2C9, quinidine for 2C19, ticlopidine for 2D6, and ketoconazole for 3A4.

Serratia arcescens. All these strains are clinically obtained and phenotypically resistant to PB (Fig. S1C). As illustrated in Fig. 2C, derivative **A22** significantly synergized PB against these species (FICI ≤0.26), except for *Proteus mirabilis*. Interestingly, when **A22** was combined with colistin (polymyxin antibiotic as well) or other classes of antibiotics, such as tobramycin, piperacillin, meropenem, ciprofloxacin rifampicin and sulfadiazine, and no synergetic activity was observed against *P. aeruginosa* DK2, except with colistin (Supporting Information Table S3 and Fig. 2D). These findings suggest that **A22** is a broad-spectrum adjuvant specifically to polymyxins against Gram-negative bacteria, providing insights into its synergistic mechanism.

3.6. *Safety, solubility, and plasma protein binding evaluation of derivative **A22***

To address the cytotoxicity concerns of compound 15, we evaluated the safety profile of derivative **A22** using two mammalian cell lines, 293 T and HUVEC. As shown in Table 3, derivative **A22** exhibited minimal cytotoxicity (IC_{50} > 150 μmol/L) in both cell lines, surpassing compound 15 (IC_{50} = 12.11 μmol/L for 293 T and IC_{50} = 18.69 μmol/L for HUVEC). Given the potential risk of cardiotoxicity associated with human ether-a-go-go (hERG) suppression[25], derivative **A22** was tested on the hERG potassium channel patch-clamp assay, with cisapride as a control. Derivative **A22** displayed an acceptable affinity for hERG (IC_{50} = 6.94 μmol/L), which is significantly lower than that of cisapride (IC_{50} = 0.036 μmol/L, Supporting Information Fig. S2), indicating a lower cardiotoxicity risk.

In addition, **A22** exhibited improved water solubility (4 μg/mL) compared to compound 15, as well as high plasma protein binding (PPB) potential (97.94%), suggesting a long maintenance time and stable effect *in vivo* (Table 3). These results indicate that derivative **A22** has a favorable safety profile *in vitro* and improved bioavailability.

3.7. *Metabolic stability evaluations of derivative **A22***

We conducted a stability assay in human liver microsomes (HLM) and mouse liver microsomes (MLM), using verapamil as a control. As presented in Table 4, derivative A22 demonstrated reasonable metabolic stability, with a half-life ($t_{1/2}$) of 29.09 min

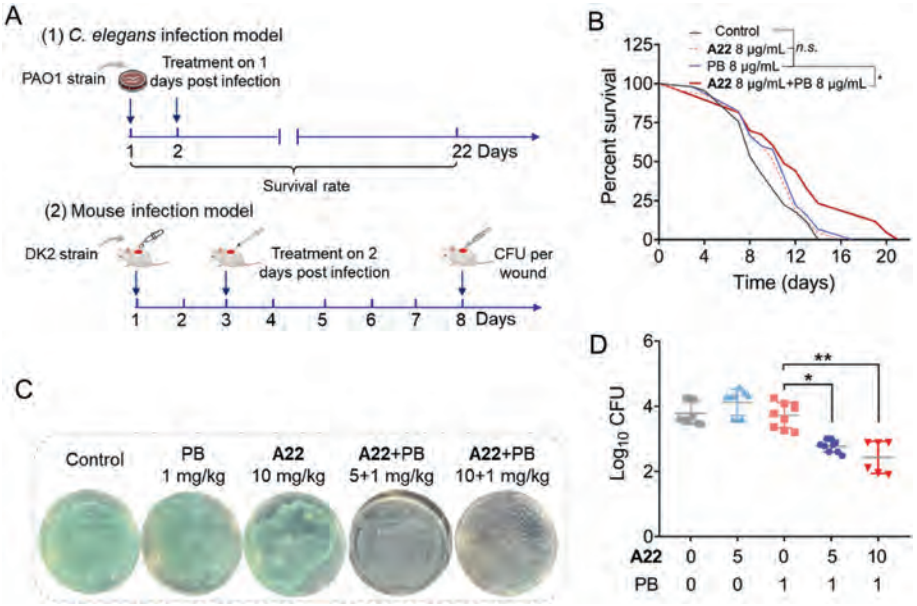

Figure 3 *In vivo* potency of derivative **A22** in *C. elegans* and mouse. (A) Schematic representation of the experimental protocol for *C. elegans* and mouse infection models; (B) Survival curves of PAO1-infected N2 worms (n = 2, 20−25 worms/well); (C, D) Bacterial load in the mice wound infection model. Data are presented as mean ± SD of three independent experiments. *P < 0.05, **P < 0.01, *n.s.* = no significance. Statistical comparisons were performed using the Long-rank (Mantel−Cox) test for *C. elegans* infection model and one-way ANOVA for mouse wound infection model.

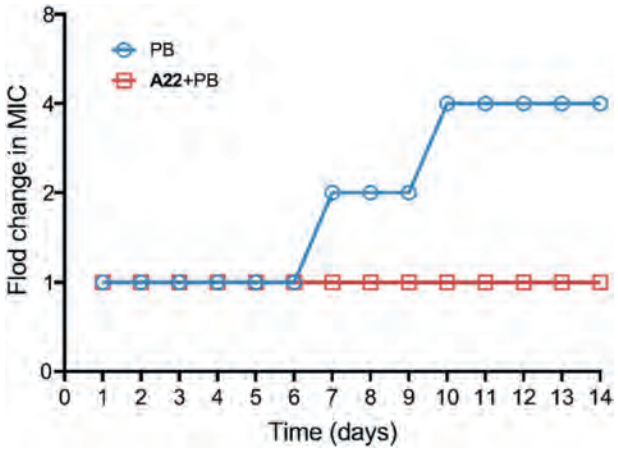

Figure 4 Development of bacterial resistance in *P. aeruginosa* DK2 during monotherapy of PB or combination therapy with **A22**.

in HLM and 54.43 min in MLM, showing 23.96% and 46.31% of the compound remaining after 1 h, respectively. These results suggest that derivative **A22** possessed adequate metabolic stability, further supporting its potential as a drug candidate.

3.8. *The inhibition of human CYP450 enzymes of derivative **A22***

As shown in Table 5, **A22** exhibited moderate inhibition of CYP2C8, CYP2C9, and CYP2D6 with IC_{50} values of 2.61, 0.29 and 1.88 μmol/L, respectively. Moreover, **A22** demonstrated minimal inhibition against CYP1A2, CYP2B6, CYP2C19, and CYP3A with IC_{50} values of 6.13, >33.00, 20.5, and >33.00 μmol/L, respectively. This profile suggests a low risk of drug−drug interactions from **A22**.

3.9. *In vivo synergetic potency of derivative **A22***

Given the potent synergistic activity, favorable safety profile, and adequate metabolic stability of derivative **A22**, we further conducted *in vivo* pharmacodynamic studies. First, *Caenorhabditis elegans* (*C. elegans*) was infected with *P. aeruginosa* PAO1 and treated with the monotherapy or combinational therapy of derivative **A22** and PB (Fig. 3A and B). The results demonstrated that neither **A22** nor PB had significant therapeutic effects on the survival of the worms. Whereas the combination of 8 μg/mL **A22** and 8 μg/mL PB synergistically extended the lifespan of the worms, demonstrating the efficacy of the combination therapy *in vivo*.

Next, the therapeutic potential of **A22** was evaluated in a mouse wound infection model infected with *P. aeruginosa* DK2. Excisional wounds were created on the dorsal region of the mice on day 1, followed by *P. aeruginosa* DK2 infection. Treatment began on day 2 post-infection to allow sufficient time for wound colonization (Fig. 3A). As shown in Fig. 3C and D, neither **A22** monotherapy (10 mg/kg) nor PB monotherapy (1 mg/kg) exhibited significant antibacterial effects after 7 days of treatment. In stark contrast, the combinational therapy of **A22** (10 mg/kg) and PB (1 mg/kg) significantly reduced bacterial loads in the infected wounds compared to control and monotherapy, effectively clearing the infection.

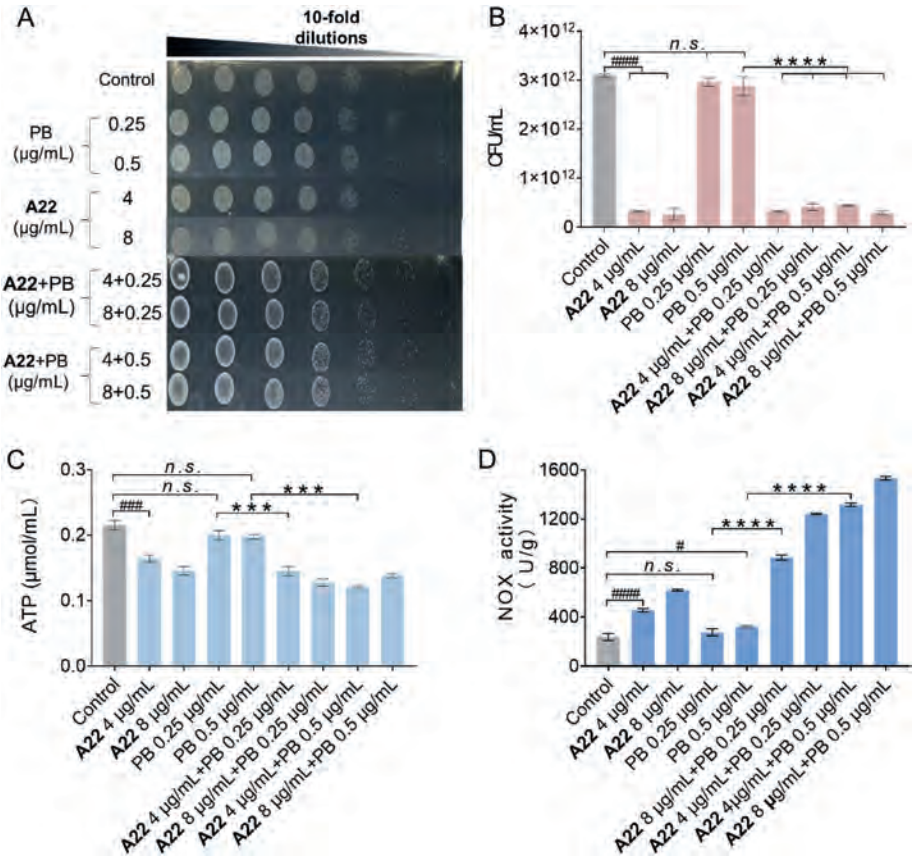

Figure 5 Antioxidant effects on *P. aeruginosa* DK2. (A) Each spotted on LB solid plates; (B) Statistical graph of CFU counts; (C) ATP levels; (D) NOX activity. Data are presented as means ± standard deviation of three independent experiments. $^{\#}P < 0.05$, $^{\#\#}P < 0.01$, $^{\#\#\#}P < 0.001$, $^{\#\#\#\#}P < 0.0001$, *n.s.* = no significance, as compared to the control group. $^{**}P < 0.01$; $^{***}P < 0.001$; $^{****}P < 0.0001$, as compared to the PB alone group. Statistical comparisons were performed using one-way ANOVA.

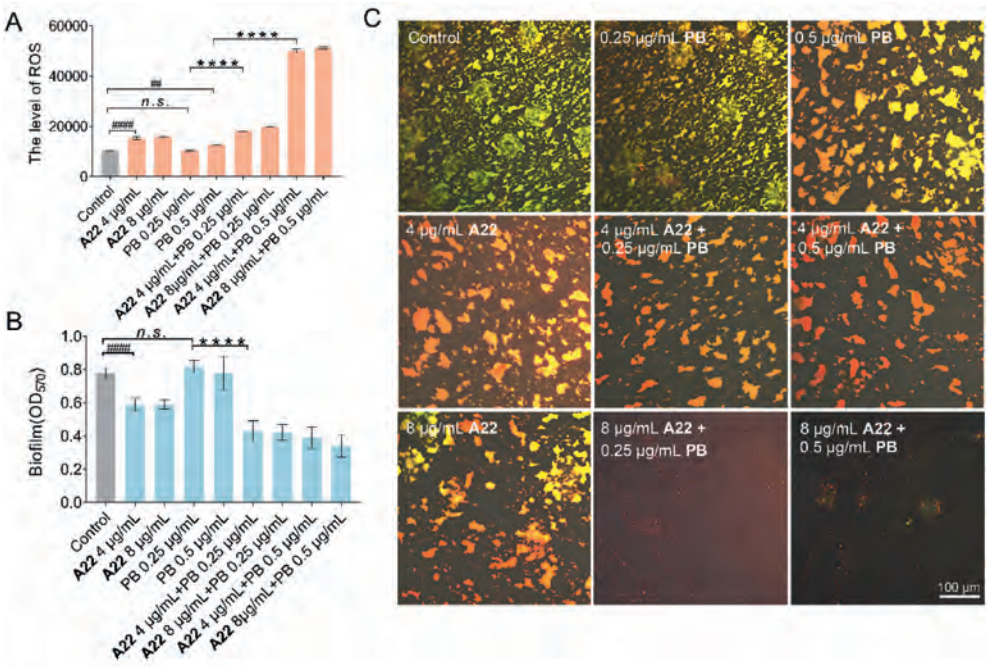

Figure 6 (A) ROS levels at different concentrations of the derivative **A22** alone and in combination; (B) Inhibition of biofilm formation by different concentrations of derivative **A22** or PB alone, or in combination; (C) CLSM images of *P. aeruginosa* DK2 biofilms by different concentrations of derivative **A22** alone and in combination. Data are presented as means ± standard deviation of three independent experiments. $^{\#\#}P < 0.01$, $^{\#\#\#\#}P < 0.0001$, *n.s.* = no significance, as compared to the control group. $^{****}P < 0.0001$, as compared to the PB alone group. Scale bars = 100 μm. Statistical comparisons were performed using one-way ANOVA.

*3.10. Induction of resistance of derivative **A22***

The development of drug resistance is a major challenge in the advancement of novel antibiotics. To evaluate the ability of **A22** to suppress resistance development to PB in *P. aeruginosa* DK2 under selective pressure, a resistance induction experiment was conducted. DK2 was cultured daily in the presence of subinhibitory concentrations of PB, with or without combination treatment with **A22**, and the minimum inhibitory concentration (MIC) of PB was measured for both groups over 14 days to monitor resistance progression. As shown in Fig. 4, the group treated with PB alone (64 μg/mL) displayed a significant increase in resistance over time. The MIC of PB increased 4 folds, from 256 μg/mL at the start to 1024 μg/mL after 14 generations, clearly indicating substantial resistance development. In stark contrast, the group treated with a combination of **A22** (10 μmol/L = 3.67 μg/mL) and PB (0.5 μg/mL) exhibited no resistance development, with the MIC of PB remaining stable at 1 μg/mL (combined with 10 μmol/L **A22**) throughout the 14-day period, matching the MIC of the initial generation (Table 2).

These findings demonstrate that **A22** effectively prevents the emergence of PB resistance in *P. aeruginosa* DK2, aligning with the design rationale for adjuvants to combat bacterial resistance, and highlighting **A22**'s potential as a promising adjuvant for improving the efficacy and longevity of polymyxin-based therapies.

*3.11. Synergistic mechanism of derivative **A22***

Previous results from *Section 2.5* demonstrated that derivative **A22**'s mechanism of synergism is closely related to the mode of action of polymyxins, which primarily disrupt bacterial membranes by binding to lipopolysaccharides (LPS) on the outer membrane. The disruption of the bacterial outer membrane compromises membrane integrity, leading to increased permeability and subsequent membrane depolarization. This process not only weakens the bacterial cell wall but also perturbs the proton motive force (PMF), which is essential for ATP production and homeostasis in bacteria[26,27]. The resulting cellular damage from membrane disruption likely triggers a cascade of stress responses, including the activation of oxidative stress pathways[28]. Given this membrane destabilization and the associated stress, we hypothesized that **A22** amplifies polymyxin-induced bactericidal effects by modulating oxidative stress responses in *P. aeruginosa* DK2.

To investigate this hypothesis, *P. aeruginosa* DK2 was treated with PB (0.25 or 0.5 μg/mL), the lead compound 15, and derivative **A22** (4 or 8 μg/mL). Antioxidant capacity was assessed by observing *P. aeruginosa* DK2 growth under oxidative stress (H_2O_2) environments. PB alone did not reduce CFU, whereas treatment with either the lead compound 15 or derivative **A22**, with or without PB, significantly reduced CFU (Fig. 5A and B and Supporting Information Fig. S3A). These above results indicated derivative **A22** significantly decreases the antioxidant capacity of *P. aeruginosa* DK2. This hypothesis is further supported by ATP level measurements. Monotherapy with 15 or **A22** reduced ATP levels in *P. aeruginosa* DK2, consistent with PMF dissipation, and the reduction in ATP levels was even more pronounced when combined with PB (Fig. 5C and Fig. S3B). Additionally, NOX activity, which reflected ROS generation[29], was significantly increased by both 15 and **A22**, with a further significant increase in combination with PB (Fig. 5D and Fig. S3C).

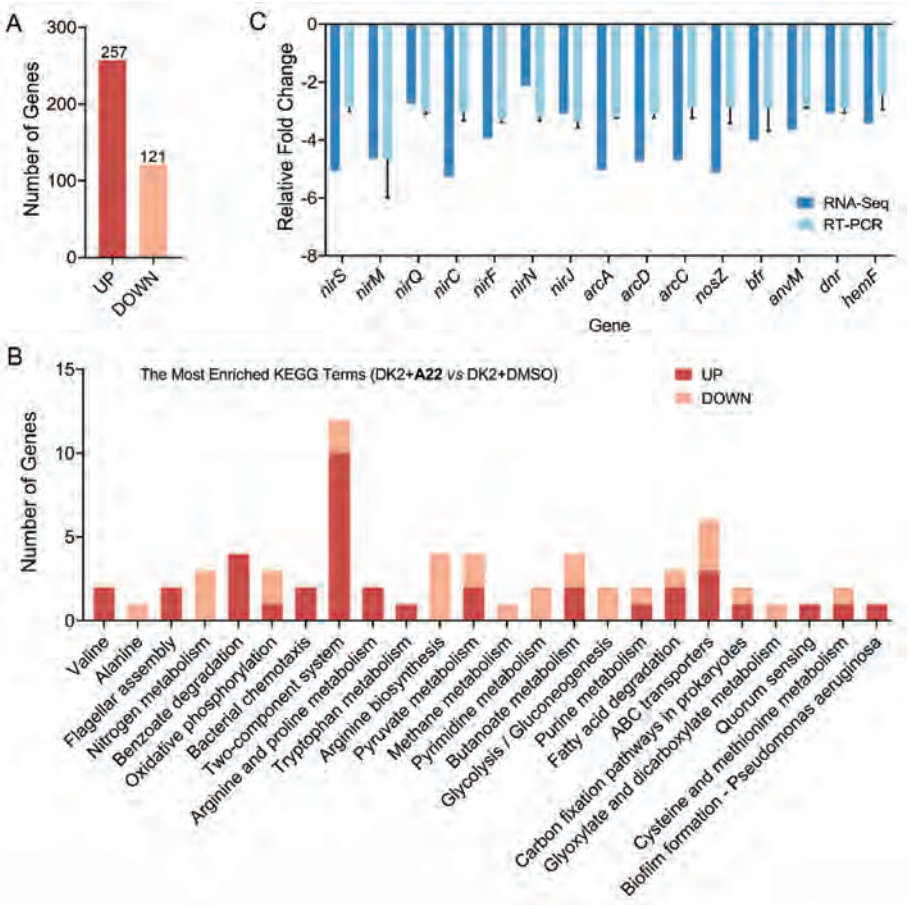

Figure 7 Differential gene expression profiles caused by derivative **A22** in *P. aeruginosa* DK2. (A) Up- and down-regulation of genes in response to derivative **A22** compared to control; (B) KEGG term enrichment analysis of differentially expressed genes; (C) RNA-seq and qRT-PCR analysis of representative genes.

Direct measurement of ROS levels confirmed these results, with both 15 and derivative **A22** significantly elevating ROS levels, and **A22** demonstrating a more pronounced effect than 15, especially in combination with PB (Fig. 6A and Fig. S3D). The relationship between oxidative stress and antibiotic resistance in *P. aeruginosa* is well-established, influencing not only efflux pump gene expression but also biofilm formation, a critical virulence factor often links to antimicrobial resistance[30−34].

As shown in Fig. 6B and C, **A22** exhibited potent inhibitory activity against biofilm formation in *P. aeruginosa* DK2 at both 4 and 8 μg/mL, as evidenced by crystal violet staining and confocal laser scanning microscopy (CLSM) images. Notably, the inhibitory effect was significantly enhanced when 8 μg/mL **A22** was combined with either 0.25 or 0.5 μg/mL PB, demonstrating a robust synergy in disrupting biofilm-associated bacterial defenses.

Together, these findings suggest that **A22** enhances the bactericidal effect of polymyxins by reducing *P. aeruginosa* DK2's antioxidant capacity, facilitating ROS accumulation, disrupting the PMF, inhibiting biofilm formation, and ultimately leading to bacterial death. This oxidative stress modulation is a key mechanism by which **A22** selectively synergizes polymyxins.

*3.12. Gene expression modulated by derivative **A22***

To elucidate the impact of derivative **A22** on *P. aeruginosa* DK2, we conducted a transcriptomic analysis using RNA sequencing (RNA-Seq) to compare the gene expression profiles of the **A22**-treated group with the control group. Differential gene expression analysis revealed that 257 genes were upregulated and 121 genes were downregulated (Log_2 fold change $\geq$2.0, Fig. 7A and Supporting Information Table S4). These differentially expressed genes are involved in various resistance-related functions, including the two-component regulatory system, oxidative phosphorylation, nitrogen metabolism, bacterial chemotaxis, amino acid metabolism, pyruvate metabolism, butyrate metabolism, fatty acid degradation, and ABC transporters (Fig. 7B and Table S4).

To validate the RNA-Seq results, quantitative RT-PCR was performed on selected genes (Fig. 7C). The analyzed genes included those related to the denitrification nir system (*nirS*, *nirM*, *nirC*, *nirF*, *nirN*, and *nirJ*), arginine metabolism (*arcA*, *arcD*, and *arcC*) and oxidative stress related genes (*nosZ*, *bfr*, *anvM*, *dnr*, and *hemF*). AnvM acts as an anaerobic toxicity regulator, contributing to oxidative stress response, redox enzyme activity, transcription regulation, exercise, and pathogenicity[35]. HemF is an oxygen-dependent cytochrome III oxidase that plays a certain role in oxygen metabolism[36]. The nir system regulates nitrite metabolism pathways and modulates nitric oxide (NO) levels, which are crucial for the increased activity of KatA[37].

The transcriptome data also verified our previous experimental results and the antioxidative stress-related genes were also significantly down-regulated after derivative **A22** treatment, which further suggests that derivative **A22** may synergize PB through the

oxidative stress pathway. However, we also found that derivative **A22** also affects a number of pathways associated with drug resistance, and it is possible that there are multiple targeting pathways of action for derivative **A22** to synergize polymyxins. There is still a long way to go to study the synergistic mechanism of derivative **A22**, and in the future, we will focus more on the identification and study of direct targets.

4. Conclusions

In this study, we successfully synthesized and evaluated a series of novel benzamide derivatives for their ability to synergize polymyxins against MDR *P. aeruginosa* DK2. Among these, derivative **A22** emerged as a particularly promising candidate, demonstrating superior synergistic activity to PB *in vitro*, while exhibiting no inherent antibacterial activity. Compared to the lead compound 15, **A22** showed significantly lower cytotoxicity toward mammalian cells, improved solubility, and exhibited reasonable metabolic stability. Notably, **A22** broadly potentiated polymyxins against various clinically isolated MDR Gram-negative strains. Furthermore, **A22** demonstrated potent *in vivo* efficacy in both *C. elegans* and mouse infection models, further supporting its potential as a safe and effective adjuvant. Resistance assay indicated combination treatments with derivative **A22** and PB significantly suppressed resistance development in *P. aeruginosa* DK2 compared to PB single treatment. Mechanistic studies revealed that **A22** effectively reduces antioxidant capacity, diminishes ATP production, dissipates the PMF, increases NOX activity, elevates ROS levels, and inhibits biofilm, leading to a cascade of events that culminates in bacterial death. These findings suggest that **A22** is a promising candidate for further clinical development as an adjuvant for polymyxin-based therapies, offering a valuable approach to combating MDR bacterial infections.

Acknowledgments

This work was financially supported by the National Natural Science Foundation of China (No. 22107023 and 32300033), the Natural Science Foundation of Hainan (No. 222QN220, China), and the Scientific Research Foundation of Hainan University (No. KYQD(ZR)-22010 and KYQD(ZR)-23006, China).

Author contributions

This study was initiated and designed by Baoli Li, Shihao Song, and Jian Li. Taotao Lu, Chaohui Wu, and Qian Li synthesized the compounds and evaluated their synergistic activity. Hongguang Han conducted the biological evaluation and mechanism studies. Hongyan Hu, Wenwen Liu, Donglei Shi, Feifei Chen, and Lefu Lan provided reagents, materials, and analysis tools. Data analysis and interpretation were carried out by Baoli Li, Shihao Song, and Jian Li. The manuscript was written by Taotao Lu, Baoli Li, and Shihao Song. All of the authors have read and approved the final manuscript.

Conflicts of interest

The authors have no conflicts of interest to declare.

Appendix A. Supporting information

Supporting information to this article can be found online at https://doi.org/10.1016/j.apsb.2025.01.022.

References

1. O'Neill J. *Tackling drug-resistant infections globally: final report and recommendations*. Government of the United Kingdom; 2016.
2. Kalan L, Wright GD. Antibiotic adjuvants: multicomponent anti-infective strategies. *Expert Rev Mol Med* 2011;**13**:e5.
3. Chakradhar S. Reservoirs of resistance: to understand why antibiotics fail, geneticists chase the 'resistome'. *Nat Med* 2016;**22**: 1069−71.
4. Melander RJ, Melander C. The challenge of overcoming antibiotic resistance: an adjuvant approach?. *ACS Infect Dis* 2017;**3**:559−63.
5. Dhanda G, Acharya Y, Haldar J. Antibiotic adjuvants: a versatile approach to combat antibiotic resistance. *ACS Omega* 2023;**8**: 10757−83.
6. Wright GD. Antibiotic adjuvants: rescuing antibiotics from resistance. *Trends Microbiol* 2016;**24**:862−71.
7. Douafer H, Andrieu V, Phanstiel OIV, Brunel JM. Correction to antibiotic adjuvants: make antibiotics great again. *J Med Chem* 2020; **63**:1440.
8. Rossi E, La Rosa R, Bartell JA, Marvig RL, Haagensen JAJ, Sommer LM, et al. *Pseudomonas aeruginosa* adaptation and evolution in patients with cystic fibrosis. *Nat Rev Microbiol* 2021;**19**:331−42.
9. Jurado-Martín I, Sainz-Mejías M, McClean S. *Pseudomonas aeruginosa*: an audacious pathogen with an adaptable arsenal of virulence factors. *Int J Mol Sci* 2021;**22**:3128.
10. Blomquist KC, Nix DE. A Critical Evaluation of newer β-Lactam antibiotics for treatment of *Pseudomonas aeruginosa* infections. *Ann Pharmacother* 2021;**55**:1010−24.
11. Folkesson A, Jelsbak L, Yang L, Johansen HK, Ciofu O, Høiby N, et al. Adaptation of *Pseudomonas aeruginosa* to the cystic fibrosis airway: an evolutionary perspective. *Nat Rev Microbiol* 2012;**10**: 841−51.
12. Lu TT, Zheng XY, Mao F, Cao Q, Cao Q, Zhu J, et al. Novel niclosamide-derived adjuvants elevating the efficacy of polymyxin B against MDR *Pseudomonas aeruginosa* DK2. *Eur J Med Chem* 2022; **236**:114318.
13. Livak KJ, Schmittgen TD. Analysis of relative gene expression data using real-time quantitative PCR and the 2(-Delta Delta C(T)) Method. *Methods* 2001;**25**:402−8.
14. Zheng RP, Feng XM, Wei XY, Pan XL, Liu C, Song RP, et al. PutA is required for virulence and regulated by prur in *Pseudomonas aeruginosa*. *Front Microbiol* 2018;**9**:548.
15. Beutler E, Mathai CK. A comparison of normal red cell ATP levels as measured by the firefly system and the hexokinase system. *Blood* 1967;**30**:311−20.
16. Kawai S, Mori S, Mukai T, Murata K. Cytosolic NADP phosphatases I and II from Arthrobacter sp. strain KM: implication in regulation of NAD^+/$NADP^+$ balance. *J Basic Microbiol* 2004;**44**: 185−96.
17. Jia SJ, Jiang DJ, Hu CP, Zhang XH, Deng HW, Li YJ. Lysophosphatidylcholine-induced elevation of asymmetric dimethylarginine level by the NADPH oxidase pathway in endothelial cells. *Vasc Pharmacol* 2006;**44**:143−8.
18. Yao J, Allen C. The plant pathogen *Ralstonia* solanacearum needs aerotaxis for normal biofilm formation and interactions with its tomato host. *J Bacteriol* 2007;**189**:6415−24.
19. Cheng WJ, Zhou JW, Zhang PP, Luo HZ, Tang S, Li JJ, et al. Quorum sensing inhibition and tobramycin acceleration in *Chromobacterium violaceum* by two natural cinnamic acid derivatives. *Appl Microbiol Biotechnol* 2020;**104**:5025−37.
20. Langmead B, Salzberg SL. Fast gapped-read alignment with Bowtie 2. *Nat Methods* 2012;**9**:357−9.
21. Trapnell C, Williams BA, Pertea G, Mortazavi A, Kwan G, van Baren MJ, et al. Transcript assembly and quantification by RNA-Seq reveals unannotated transcripts and isoform switching during cell differentiation. *Nat Biotechnol* 2010;**28**:511−5.
22. Zeng R, Lu TT, Wu LY, Zhang Q, Shi DL, Li J, et al. Structural modification and activity evaluation of sensitizers against

drug-resistant *Pseudomonas aeruginosa* DK2. *J Shenyang Pharm Univ* 2023;**40**:1587−97.
23. Xu JM, Ai J, Liu SY, Peng X, Yu LQ, Geng M, et al. Design and synthesis of 3,3'-biscoumarin-based c-Met inhibitors. *Org Biomol Chem* 2014;**12**:3721−34.
24. Odds FC. Synergy, antagonism, and what the chequerboard puts between them. *J Antimicrob Chemother* 2003;**52**:1.
25. Garrido A, Lepailleur A, Mignani SM, Dallemagne P, Rochais C. hERG toxicity assessment: useful guidelines for drug design. *Eur J Med Chem* 2020;**195**:112290.
26. Vranas M, Wohlwend D, Qiu D, Gerhardt S, Trncik C, Pervaiz M, et al. Structural basis for inhibition of ROS-producing respiratory complex I by NADH-OH. *Angew Chem Int Ed* 2021;**60**:27277−81.
27. Glasser NR, Kern SE, Newman DK. Phenazine redox cycling enhances anaerobic survival in *Pseudomonas aeruginosa* by facilitating generation of ATP and a proton-motive force. *Mol Microbiol* 2014;**92**: 399−412.
28. Van Acker H, Coenye T. The role of reactive oxygen species in antibiotic-mediated killing of bacteria. *Trends Microbiol* 2017;**25**: 456−66.
29. Gong HR, Li J, Xu A, Tang YT, Ji WX, Gao RG, et al. An electron transfer path connects subunits of a mycobacterial respiratory supercomplex. *Science* 2018;**362**:eaat8923.
30. Xia B, Li M, Tian ZY, Chen GK, Liu C, Xia YS, et al. Oligoribonuclease contributes to tolerance to aminoglycoside and β-lactam antibiotics by regulating KatA in *Pseudomonas aeruginosa*. *Antimicrob Agents Chemother* 2019;**63**:e00212-19.
31. García-Contreras R, Nuñez-López L, Jasso-Chávez R, Kwan BW, Belmont JA, Rangel-Vega A, et al. Quorum sensing enhancement of the stress response promotes resistance to quorum quenching and prevents social cheating. *ISME J* 2015;**9**:115−25.
32. Xia YS, Cebrián R, Xu CJ, Jong A, Wu WH, Kuipers OP. Elucidating the mechanism by which synthetic helper peptides sensitize *Pseudomonas aeruginosa* to multiple antibiotics. *Plos Pathog* 2021;**17**:e1009909.
33. da Cruz Nizer WS, Inkovskiy V, Versey Z, Strempel N, Cassol E, Overhage J. Oxidative stress response in *Pseudomonas aeruginosa*. *Pathogens* 2021;**10**:1187.
34. Balasubramanian D, Schneper L, Kumari H, Mathee K. A dynamic and intricate regulatory network determines *Pseudomonas aeruginosa* virulence. *Nucleic Acids Res* 2013;**41**:1−20.
35. Zhang YC, Zhou CM, Pu QQ, Wu Q, Tan SR, Shao XL, et al. *Pseudomonas aeruginosa* regulatory protein AnvM controls pathogenicity in anaerobic environments and impacts host defense. *mBio* 2019;**10**:e01362-19.
36. Breckau D, Mahlitz E, Sauerwald A, Layer G, Jahn D. Oxygen-dependent coproporphyrinogen III oxidase (HemF) from *Escherichia coli* is stimulated by manganese. *J Biol Chem* 2003;**278**:46625−31.
37. Su SC, Panmanee W, Wilson JJ, Mahtani HK, Li Q, Vanderwielen BD, et al. Catalase (KatA) plays a role in protection against anaerobic nitric oxide in *Pseudomonas aeruginosa*. *PLoS One* 2014;**9**:e91813.